Pierced Sensor for a Nano-Microscope (NMSC)

R. Sklyar

Verchratskogo st. 15-1, Lviv 79010 Ukraine, sklyar@tsp.lviv.ua

ABSTRACT

A nanoSuFET with a high-temperature superconducting channel is introduced into the tissue or material for transducing their signals in both directions. The microwave imaging process is based on the nanowire or CNT exciting/ pickup coil. The equation for computations of the coils' RLC values on UHF are presented. The sensitivity of this nano-microscope can be estimated as $H_J = 10^{-4}$ (A·m/√Hz) with SNR equal to 10^4. The sensitivity of an advanced first-order biogradiometer is equal to 3fT/√Hz. The smallest change in magnetic moment detected by this system in the band 10 Hz is 1 fJ/T.

Keywords: magnetic field, eddy current, exciting/pickup coil, SuFET, nanowire, CNT, polymer FET, gradiometer

1 INTRODUCTION

A miniaturized niobium based DC superconducting quantum interference device (SQUID) magnetometer for high magnetic field (MF) sensitivity applications has been developed. The sensing coil consists of an integrated square superconducting coil with a length of 3 mm, involving a device area much smaller with respect to the standard SQUID magnetometers with a comparable MF sensitivity; so it allows increasing the spatial resolution keeping the MF sensitivity unaltered [1]. Furthermore, a small pickup coil (PC) minimizes its antenna gain, reducing the radio frequency interference. At T=4.2K, the sensors have shown smooth and resonance free V-Phi characteristics and an intrinsic white MF noise spectral density as low as 5.8 fT/ $Hz^{1/2}$, measured in flux locked loop configuration. Due to their compactness and good characteristic parameters, such sensors are suitable for large multichannel systems used in biomagnetic imaging.

A detection system for eddy current testing (ECT) utilizing a normal PC cooled at T j 77K and a picovoltmeter based on a high-Tc SQUID has been developed [2]. In this system, the PC is located in an unshielded environment, whereas the voltage across the coil is detected with the SQUID picovoltmeter placed in a small magnetic shield. It was shown that the coil could be moved in the unshielded environment without the degradation of its performance (Fig. 1). By moving the coil, we successfully detected a small crack on the back surface of a Cu plate in an unshielded environment.

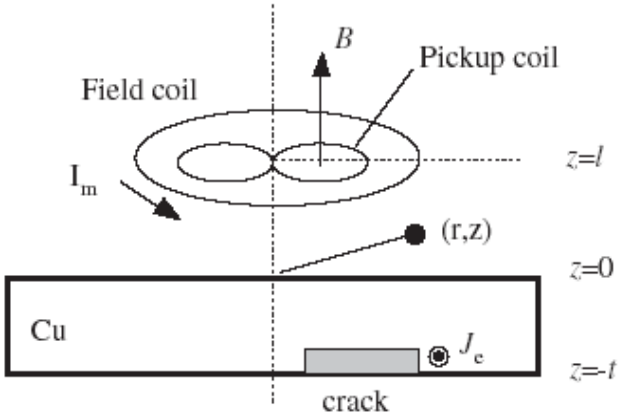

Figure 1: Geometry used in eddy current analysis.

2 MAGNETIC NANO-MICROSCOPE

A new design for scanning or sounding micro- or nanoscopes combines a simple mechanical arrangement with a miniature ***exciting/PC (EC/PC)*** of the **superconducting induction magnetometer (SIM)** [3]. The microwave imaging process (Fig. 2) is shown on a prototype sample: a normal conducting ring of self-inductance L_i and resistance R_i. The quantity L_0 is the PC self-inductance and MI_i represents the magnetic coupling of PC through a mutual inductance M to an external circuit carrying a current I_i in the material or tissue. If $\omega_T >> R_i L_i$, then R_i may be ignored and $I_i(\omega_T) \approx - I_j(\omega_T) M/L_i$.

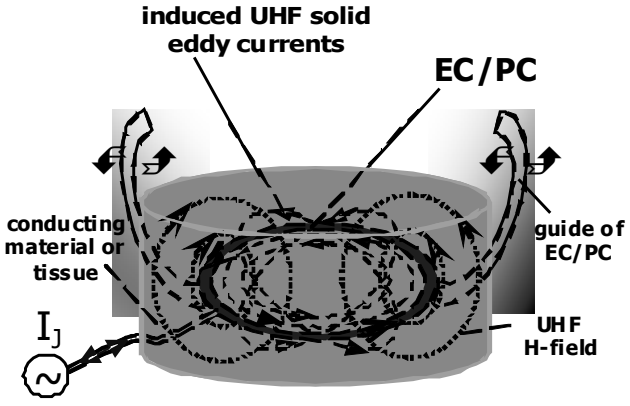

Figure 2: Schematic diagram of SIM based MNSC.

An interesting structure is that of helical carbon nanotubes (CNTs), or nanocoils for EC/PC (Fig. 3, a). Nanocoils offer unique electronic properties that straight CNTs do not have. The plasticity of CNTs will be relevant to their use in nanoscale devices [4].

3 APPLICATION OF THE NANOWIRE AND POLYMER EC/PC WITH FETS

For nonzero drain voltages the **superconducting field-effect transistor (SuFET)** absorbs low- frequency power of the average Josphson current I_J and re-emits this power at extremely high frequencies. The feasibility of the transistor function on a yarn-like structure has been demonstrated (Fig. 3, b) [5]. As a result, the decreasing of the SuFET channel's current is defined by the value of losses for eddy currents $I_i(\omega_T)$ in the tissue:

$$\Delta I_J(\omega_T) = I_J(\omega_T) - I_i(\omega_T) = K_J\left(\frac{V_{DS}}{2} - V_{GS}\right)\left(1 - \frac{M}{L_i}\right) \quad (1)$$

Thus, by monitoring the change in $\Delta I_j(\omega_T)$ as a function of PC position, we make use of the factor M/Li dynamics of the tissue to obtain a micro- or nanowave screening image.

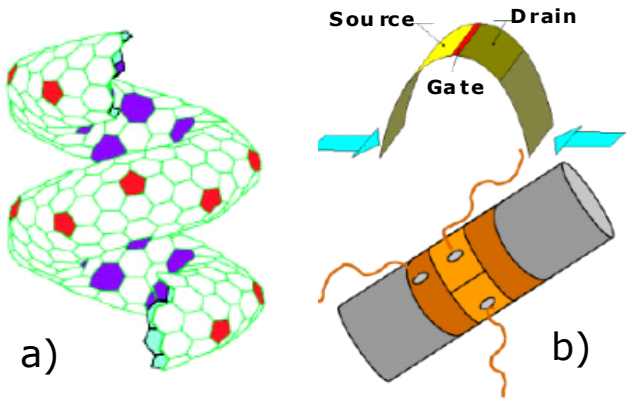

Figure 3: Application of the nanowire and polymer elements- a) a helical CNT tube; b) an e-yarn.

One-dimensional nanowires are destined to play an important role in FETs and their potential applications in various fields [6]. Among these materials, ZnO nanowires have been intensively investigated because of their simple synthetic procedure and high crystalline quality. Recently, flexible and transparent substrates have gained increasing attention in the semiconductor industry, due to their lightweight and the facility they provide for fabricating electronic devices.

Composites of semiconductive polymers and single-walled carbon nanotubes (SCNTs) and their application to organic FETs has been studied [7]. Figure 4 shows by enhancement of FET mobility incorporation of SCNT-complex into semiconductive polymers.

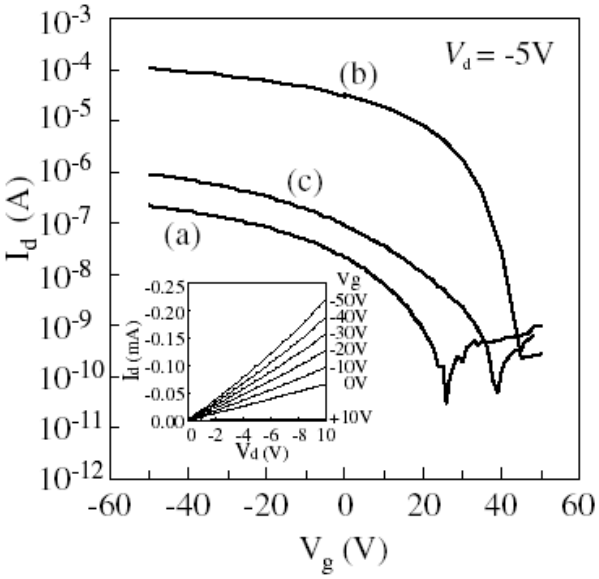

Figure 4: I_d vs V_g of thin-film FET made of P3HT and its composite with SCNT-complex. The inset shows the I_d vs V_d.

3.1 EC/PC Based on Smart Textiles

Hence the mechanical stability of the smart textiles is sufficient for implantation of the planar structures (Fig. 5). Since the developed system allow the micro- and nanoscopic of room and tissue temperature samples, such testing will be of practical use for clinical diagnostic.

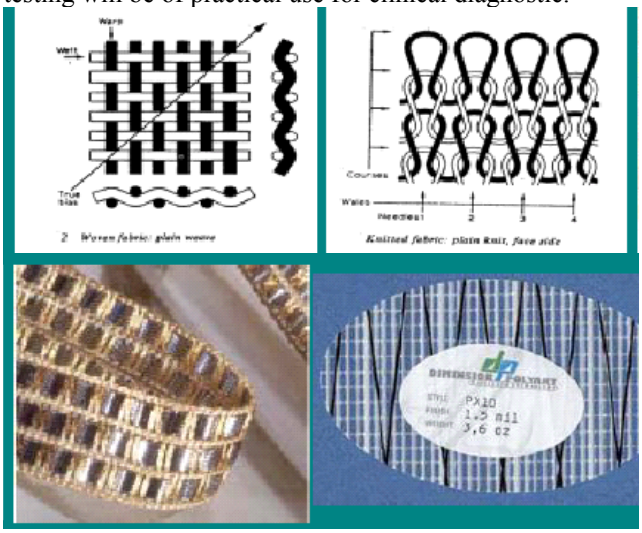

Figure 5: Textile sensor network.

The sensitivity of this instrument H_J can be estimated by considering the noise source I_{NJ} of SuFET according. The digital value of H_J for PC with the diameter of 0.1 μm and inductance 1 μH, and $I_{NJ}=10^{-11}$ (A·Hz) is equal to: $H_J=I_{NJ}L/\mu_0 S_{eq}=10^{-4}$ (A·m/√Hz). This means that with a SIM exciting signal $H_{sign}=(V_{DS}/2-V_{GS})/\mu_0 S_{eq}\omega_T=(V_{DS}/2-V_{GS})\cdot 10^3\approx$

NSTI-Nanotech 2009, www.nsti.org, ISBN 978-1-4398-1782-7 Vol. 1, 2009

1 (A·m) a magnetic SNR in a band less than 10 Hz will be: $H_{sign}/H_R(\Delta 10Hz)=(V_{DS}/2-V_{GS})/ I_{NJ}L\omega_T$. For the said values, SNR of the described NMSC will be equal to $H_{SNR}=(V_{DS}/2-V_{GS})\cdot 10^7 \approx 10^4$. Typically our magnetic images are taken at about 8 pixels/s.

4 DESIGN VARIANTS OF A SENSOR

To achieve a high spatial resolution, our nano-microscope (NMSC) uses a small ambient temperature PC(s) directly as a magnetic sensor, rather than a SQUID's pickup loop coupled to a cooled SuFET. Sounding and scanning closer to the tissue improves the spatial resolution, thanks to the complete penetration into the measuring process. Other than the SuFET itself, there are no other microwave components, sources, or detectors. This is particular advantageous at very high frequencies where components are difficult to construct. In conclusion, we note that the ability to detect small regions of nonmagnetic conducting materials, gives the magnetic flux NMSC broad capabilities in material analysis.

4.1 Parameters of the EC/PC contour

The pierced on textile coils (Fig. 5) have an electrical equivalent as a serial cylindrical mutually opposite and parallel triangular omnidirectional coils (see Fig. 6 a and b respectively):

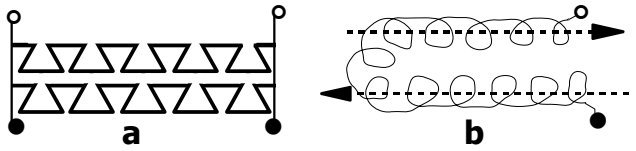

Figure 6: Equivalent circuits of a pierced EC/PCs.

In the such case, the first one is a zero-detector (where the MFs directions H of each section are compensating- Σ_H) and second n-coils MF multiplexor- $\Sigma_H=N\cdot H$. In both cases the ganging with eddy currents through the mutual inductance M will perturb that status and inductance of the investigating area of the material or tissue could be defined.

The RLC values for the cylindrical and triangular EC/PC are defined according to Eqs. 2 and 3 for their inductances respectively [8]:

$$L=\mu_0\sum_{k=1}^{n}\sum_{m=1}^{n}\int_0^{\pi} f(k,m,r_2,h_2,d_w,\varphi) \qquad (2)$$

$$L=\frac{\mu_0}{2\pi}\sum_{k=1}^{n}\sum_{m=1}^{n}\int_{x_1=0}^{(b+d_w\sqrt{3})/2}\rightarrow$$
$$\int_{x_1=-b/2}^{b/2} f(b,k,m,x_1,x_2,d_w) \qquad (3)$$

where n - a number of turns;
k, m - are sequential numbers of turns;
b, r_2, h_2, d_w - are the geometrical parameters of EC/PC;
x_1, x_2, - are reference coordinates along axis.
Also for both shapes of EC/PC on UHF by Eqs. 4 and 5:

$$R_{UHF}=\frac{l}{\pi r_0^2 \gamma}\left(\frac{1}{4}+\frac{r_0}{2z}\right) \qquad (4)$$

where $\gamma=\frac{1}{\rho}, z=(\pi\gamma\mu f)^{-1/2}$ [9]

$$C_0=\frac{4r_0 p}{(4a-\pi r_0)(n-1)\varepsilon\varepsilon_0} \qquad (5)$$

where p – a perimeter of the turn, 2a – a distance between axis of the wires, ε – a dielectrical permeability of isolation.

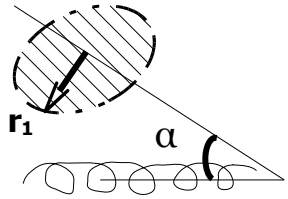

Figure 7: The geometrical model of the relative position of a one-layer EC/PC and planar contour with the crossing axis.

Furthermore, a value of M under certain relative position between between EC/PC and circular eddy current contour r_1 (Fig. 7) is defined by Eq.6, where M between a k-number EC/PC's turn and this circular contour can be calculated according to Eq.7:

$$M=\sum_{k=-n/2}^{n/2} M_{B,K} \quad \text{and} \qquad (6)$$

$$M_{B,K}=\frac{\mu_0}{2\pi}\sum_{p_1=\pm 1}\left(\int_{x_1=-b_1}^{b_2}\int_{x_2=-b_2\cos(\alpha)}^{b_2\cos(\alpha)} f(p_1,x,b,c)\right.$$
$$\left.\rightarrow+\int_{y_1=-b_1}^{b_1}\int_{y_3=0}^{b_4}\sum_{p_2=\pm 1} f(p_1,p_2,y,b,c)\right) \qquad (7)$$

where p – a summation parameter designated as 1 or -1;
c, y – are geometrical dimensions of EC/PC.

4.2 The Gradiometer Arrangement

Conventional gradiometers, such as wire-wound, thin-film, or electronic gradiometers, are axial or planar, i.e.,

‘‘one-dimensional’’ that detect the gradient of a MF in one direction. These one-dimensional gradiometers effectively reduce the ambient MF as their order increases. However, they also reduce the biomagnetic signal. A ‘‘two-dimensional’’ gradiometer detects the gradient of a MF in two orthogonal directions to achieve high SNR [10]. It focuses on a two-dimensional gradiometer that detects both the axial-second-order and planar-first-order gradients of a MF. Figure 8 shows a EC/PC for the two-dimensional gradiometer.

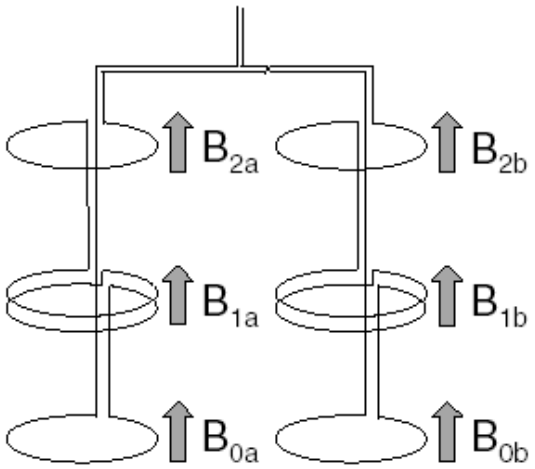

Figure 8: EC/PC for ‘‘two-dimensional’’ gradiometer that detects both axial-second-order gradient and planar-first-order gradient of MF.

Mode / Object	modulus	gradient
surface	$I_2 = \iint_S f(x,y,z) \rightarrow dxdy$	$\Delta I_2 = I_2' - I_2''$
volume	$V_2 = \iiint_V f(x,y,z)$	$\Delta V_2 = V_2' - V_2''$
structu-re level	Inside structure of the objects	Differential investigation the twin (pair) objects
object level	Inhomogeneous structure	Differential investigation the inhomogeneous twin (pair) obj.

Table 1: Dependence of the received structure parameters on the functioning mode of NMSC and possible bounds for spreading of the said method.

The described NMSC is suitable for investigating both the structure of synthetic and organic objects, and their comparing analysis (see Table 1). Following the strings of the table, investigations of biological surfaces are performing according to the surface integrals for a NMSC modulus. The same is applying to the investigations of the volumes V_1 and V_2 as the double and triple integrals respectively.

With advances in spatial resolution reaching the atomic scale, two-dimensional (2D) and 3D imaging in electron microscopy has become an essential methodology in various fields of study. A 4D imaging, with in situ spatiotemporal resolutions, in ultrafast electron microscopy (UEM) has been reported [11]. The ability to capture selected-area-image dynamics with pixel resolution and to control the time separation between pulses for temporal cooling of the specimen made possible studies of fleeting structures and morphologies by NMSC.

REFERENCES

[1] C. Granata, A. Vettoliere, and M. Russo, Appl. Phys. Lett., vol. 91, 122509 (3 pages), 2007.

[2] K. Yao, T. Q. Yang, D. Yamasaki et al., Japanese Journal of Applied Physics (JJAP), vol. 45, no. 6A, pp. 4994–4999, 2006.

[3] R. Sklyar, Journal of Automation, Mobile Robotics and Intelligent Systems (JAMRIS), vol. 1, no. 3, pp. 3-20, 2007.

[4] Yo. Nakayama, Japanese Journal of Applied Physics, vol. 46, no. 8A, pp. 5005–5014, 2007.

[5] M. Maccioni et al., Appl. Phys. Lett., vol. 89, 143515, 2006.

[6] J. Kang, K. Keem, and D.-Yo. Jeong, Japanese Journal of Applied Physics (JJAP), vol. 46, no. 9B, pp. 6227–6229, 2007.

[7] J. Tsukamoto, J. Mata, and T. Matsuno, Japanese Journal of Applied Physics (JJAP), vol. 46, no. 17, pp. L396–L398, 2007.

[8] Nemtsov M. V., “The reference book for calculation of parameters of inductance coils” (in Rus.), Moscow: Energoatomizdat, pp. 38-139, 1989.

[9] Glikman I. Ya. and Rusin Yu. S., “Calculation of the responses of radioelectronic circuits' elements” (in Rus.), Moscow: Sovetskoje radio, pp. 83-110, 1976.

[10] Yu. Seki and A. Kandori, Japanese Journal of Applied Physics (JJAP), vol. 46, no. 6A, pp. 3397–3401, 2007.

[11] B. Barwick, H. S. Park, O.-H. Kwon et al., Science, vol. 322, iss. 5905, pp. 1227-1231, 2008.